Fluid Phase Equilibria
November 2020, Volume 522, Pages 112762 (13p.)
https://doi.org/10.1016/j.fluid.2020.112762
https://archimer.ifremer.fr/doc/00642/75387/

Vapor-Liquid Equilibria, Solid-Vapor-Liquid Equilibria and H2S Partition Coefficient in (CO2 + CH4) at Temperatures Between (203.96 and 303.15) K at Pressures up to 9 MPa

Souza Lorena F.S. [1], Ghafri Saif Z.S. Al [1, 2], Fandino Torres Olivia [3], Martin Trusler J.P. [1, *]

[1] Department of Chemical Engineering, Imperial College London, South Kensington Campus, London SW7 2AZ, United Kingdom
[2] Fluid Science and Resources Division, Department of Chemical Engineering, University of Western Australia, Crawley, WA 6009, Australia
[3] Institut Français de Recherche pour l'Exploitation de la Mer (IFREMER), Centre de Bretagne, Département Ressources Physiques et Ecosystèmes de Fond de Mer, Unité des Géosciences Marines, 29280 Plouzané, France

* Corresponding author : Martin Trusler, email address : m.trusler@imperial.ac.uk

Abstract :

Vapor-liquid equilibrium (VLE) measurements of the (CO2 + CH4) system are reported along seven isotherms at temperatures varying from just above the triple point to just below the critical point of CO2 at pressures from the vapor pressure of pure CO2 to approximately 9 MPa, including near-critical states. From these data, the critical locus has been determined and correlated over its entire length. The VLE data are correlated with the Peng-Robinson equation of state (PR-EoS), using a temperature-dependent binary interaction parameter, and also compared with the predictions of the GERG-2008 equation of state. The former represents the phase compositions across all isotherms with a root-mean-square mole-fraction deviation of S = 0.0075 while, for the latter, S = 0.0126. Measurements of the three-phase solid-vapor-liquid equilibrium (SVLE) line are reported at temperatures from approximately (204 to 216) K and a new correlation is developed which is valid from 145 K to the triple point of CO2. Additionally, we report the partitioning of trace levels of H2S between coexisting liquid and vapor phases of the (CO2 + CH4) system and compare the results with the predictions of the PR-EoS.

Graphical abstract

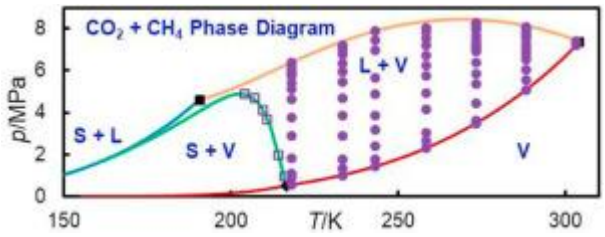

Highlight

► New vapor-liquid equilibrium data reported for CH_4 + CO_2. ► Wide temperature range, pressures up to the critical locus. ► Solid-vapor-liquid equilibrium data reported down to 204 K. ► Partition coefficient of H_2S at high dilution in CH_4 + CO_2 measured. ► Modeling with the Peng-Robinson equation of state.

Keywords : Carbon capture, transport and storage, Carbon dioxide, Equation of state, Methane, Vapor-liquid equilibrium, Phase behavior.

1. Introduction

The binary system of CO_2 + CH_4 is one of the key mixtures in gas processing and is especially important in relation to high CO_2-content natural gas processing, CO_2-enhanced gas recovery, CO_2 sequestration and hydrogen production from natural gas. The system is one of the most studied binary mixtures with at least 24 different reports on the vapor-liquid equilibrium alone. Figure 1 shows the phase diagram of the CO_2 + CH_4 system in temperature-pressure co-ordinates. This is a type 1 system with a continuous vapor-liquid critical line connecting the critical points of the pure components. A continuous solid-vapor-liquid equilibrium (SVLE) line connects the triple points of the two pure components and exhibits a pronounced maximum pressure at temperatures slightly below the CO_2 triple-point temperature. The region of the phase diagram bounded by the critical lines and the SVLE curve is of course the region within which vapor-liquid equilibrium (VLE) can occur. As shown in Fig. 1, the available experimental VLE data [1-24] cover almost all of this region. Nevertheless, there are significant discrepancies between different literature sources and no single study covers the whole of the region from the triple point temperature to the critical temperature of CO_2. For this reason, we have revisited the VLE of the (CO_2 + CH_4) system using a modern analytical apparatus.

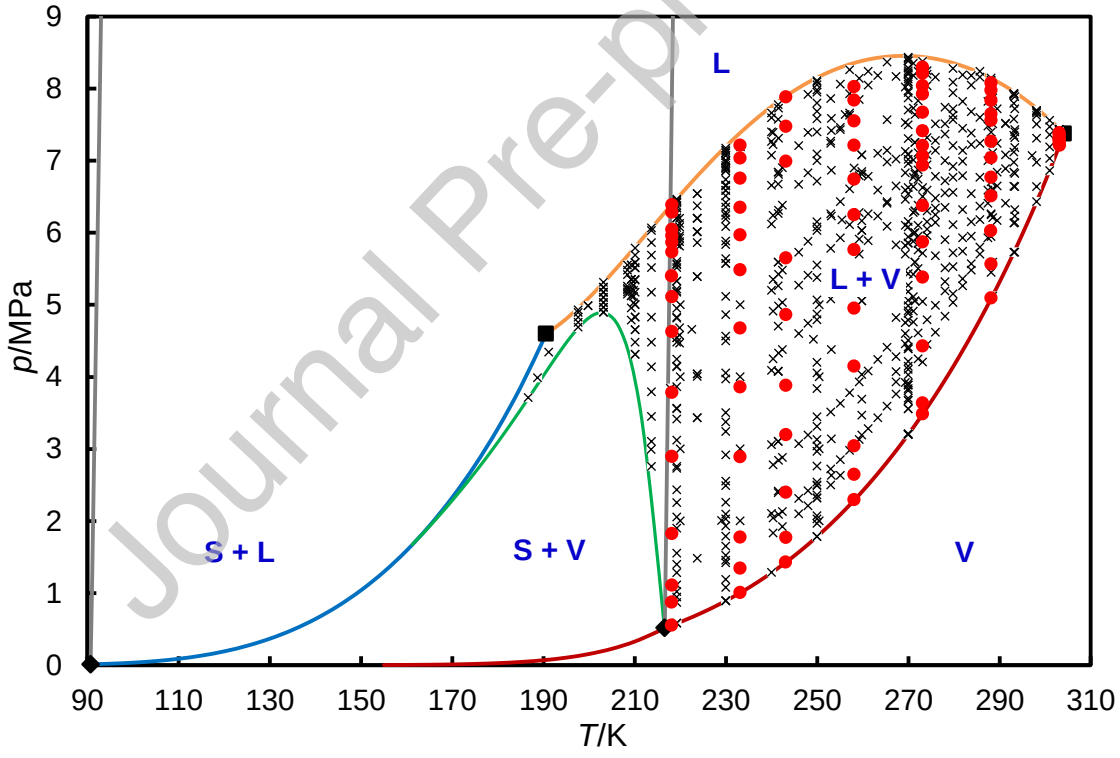

Figure 1. Phase diagram of the (CO_2 + CH_4) system where *T* is temperature and *p* is pressure. Phase boundaries are shown as solid lines: blue, vapor pressure of CH_4 [25]; red, sublimation/vapor pressure of CO_2 [26]; grey, melting curves of pure CH_4 and pure CO_2; green, three-phase solid-vapor-liquid equilibrium line (this work); orange, vapor-liquid critical curve (this work). Symbols: ◆, pure-substance triple points; ■, pure-substance critical points; ×, state points for literature VLE data [1-24]; ●; state points for VLE data reported in this work.

From a review of the literature data, it was also apparent that the path of the SVLE curve between the maximum pressure and the triple-point temperature of CO_2 had not been determined precisely. Therefore, a second objective of this study was to make new measurements of this locus.

Table 1. Summary of available experimental data for the VLE of (CO_2 + CH_4). T_{min}, T_{max}, p_{min} and p_{max} define the ranges of temperature T and pressure p for each data set.

T_{min}/K	T_{max}/K	p_{min}/MPa	p_{max}/MPa	Year	Authors	Ref.
199.8	271.5	1.48	7.91	1954	Donnelly and Katz	[1]
143.3	222.6	0.76	5.20	1959	Pikaar	[2]
277.6	277.6	6.89	6.89	1959	Robinson et al.	[3]
241.5	241.5	2.41	2.41	1964	Hensel and Massoth	[4]
233.2	283.2	5.27	8.19	1968	Kaminishi et al.	[5]
283.2	293.2	4.50	8.33	1968	Toriumi and Kaminishi	[6]
173.4	219.9	2.66	6.20	1968	Neumann and Walch	[7]
253.2	288.2	6.23	8.52	1971	Arai et al.	[8]
230.0	270.0	0.89	3.19	1976	Davalos et al.	[9]
153.2	219.3	1.19	6.49	1978	Mraw et al.	[10]
270.0	270.0	3.20	3.20	1978	Somait and Kidnay	[11]
219.3	270.0	0.58	8.42	1983	Al-Sahhaf et al.	[12]
258.2	258.2	6.90	6.90	1986	Freitag and Robinson	[13]
205.4	256.2	5.83	8.29	1989	Esper at al.	[14]
220.0	223.2	2.00	5.00	1990	Knapp et al.	[15]
288.5	293.4	5.12	8.15	1992	Xu et al.	[16]
293.0	298.1	6.02	8.04	1992	Bian	[17]
301.0	301.0	6.86	7.56	1993	Bian et al.	[18]
230.0	270.0	0.89	8.38	1995	Wei et al.	[19]
230.0	270.0	0.89	3.20	2001	Webster and Kidnay	[20]
112.0	169.9	0.09	2.32	2012	Shen et al.	[21]
277.8	302.2	4.59	7.54	2014	Ahmad et al.	[22]
240.4	297.2	1.83	8.37	2015	Nasir et al.	[23]
293.1	303.2	5.73	7.93	2018	Petropoulou et al.	[24]

Many of the gas processing scenarios mentioned above involve multi-component mixture of CH_4, CO_2 and other substances. Thermodynamic models, optimized against experimental data for binary sub-systems, are typically used to compute VLE and other properties of such systems. Toxic and corrosive acid gases, such as H_2S, OCS or SO_2, are often present under processing conditions but experimental data for mixtures containing these components are quite scares. In an effort to address this problem, we also adopted as a third objective measuring the partitioning of trace levels of H_2S between coexisting liquid and vapor phases in the (CO_2 + CH_4 + H_2S) ternary mixture. This provides very useful information, especially as H_2S is often a trace component, while allowing experiments to be carried out in a safe and reliable way.

2. Experimental

2.1 Apparatus

The apparatus used in this work has been described in detail by Fandiño et al. [27] and Souza et al. [28]. Briefly, it comprised a stainless-steel pressure vessel immersed in a refrigerated thermostatic bath and equipped with two electromagnetic sampling values (Rolsi, Evolution IV). Short capillaries (i.d. 0.13 mm) connected the sampling valves to interior of the equilibrium cell, one terminating just below the lid and the other extending almost to the bottom. The sampling valves and capillaries permitted small samples of coexisting liquid and vapor phases to be withdrawn and transferred directly to a gas chromatograph (GC) for on-line sample analysis. The vessel, of approximately 160 cm^3 volume, was fitted with a magnetic stirrer to promote equilibrium. The temperature was measured with a platinum resistance thermometer (Fluke model 5615) inserted into a thermowell bored in the wall of the vessel, and the pressure was measured with a pressure transmitter (Keller model PA-33X, 30 MPa full scale) connected in the filling line. Standard uncertainties of temperature and pressure were 0.006 K and 0.009 MPa respectively. A secondary vessel, of known volume and equipped with pressure and temperature sensors, was used to store CO_2 in a gaseous state. When initially charging the VLE cell, the CO_2 was fed from this secondary vessel and the amount admitted was estimated from the measured change in pressure, the temperature and the volume of the secondary vessel. CH_4 was admitted directly from the gas supply cylinder via a needle valve.

2.2 Materials

The gases used in this work are detailed in Table 2.

Table 2. Description of chemical samples where *x* denotes mole-fraction purity and *z* denotes mole fraction of a mixture component.

Sample	CAS Number	Source	Composition	Purity as supplied	Additional purification
Carbon dioxide	124-38-9	BOC		$x \geq 0.99995$	None
Methane	74-82-8	BOC		$x \geq 0.9995$	None
Nitrogen	7727-37-9	BOC		$x \geq 0.999992$	None
Helium	7440-59-7	BOC		$x \geq 0.99999$	None
$(1 - z)$ CO_2 + z H_2S		BOC	$z = 1 \times 10^{-3}$ [a]	$x \geq 0.999$	None
$(1 - z)$ CO_2 + z H_2S		SIP	$z = 10.0 \times 10^{-6}$ [b]	$x \geq 0.999$	None
$(1 - z)$ CO_2 + z CH_4		SIP	$z = 0.0500$ [a]	$x \geq 0.9999$	None

[a] standard uncertainty $u(z) = 0.0058z$
[b] standard uncertainty $u(z) = 0.029z$

2.3 Gas Chromatography

Composition measurements were made using a gas chromatograph (Agilent model 7890A) equipped with a thermal conductivity (TCD) and a sulfur-specific flame photometric detector (FPD). The GC was fitted with a ShinCarbon ST packed column (80/100 mesh, 2 m long x

1.0 mm ID) for measurements on the (CO_2 + CH_4) binary system, while for measurements on the (CO_2 + CH_4 + H_2S) ternary system a RT Sulfur column was used (100/120 mesh, 2 m long x 2.0 mm ID). Sulfur-inert tubing, fittings and valves were used throughout the GC system. For calibration, an internal 10-port gas-sampling valve was used. This was fitted with sample loops having nominal volumes of 0.05 mL and 0.26 mL. As described previously [27, 28], these loops were filled with calibration gases by means of filling lines equipped with pressure sensors to allow the pressure of the gas in the loop to be determined immediately prior to injection onto the column. In this work, we also added K-type thermocouples bonded onto the sample loops so as to obtain a more accurate measurement of the loop temperature. Each sample loop was equipped with two thermocouples at different points along its length and the average temperature was used. The purpose of this instrumentation was to allow the gas density in the filling loop to be calculated from an equation of state.

The primary means of calibration for the (CO_2 + CH_4) binary system was an absolute method. In this approach, the sample loops, operating at a temperature of approximately 323.15 K, were filled alternately with the pure gases to various pressures between (0.1 and 0.5) MPa. The molar density ρ_i of gas i in a filling loop was calculated from the measured temperature and pressure using a reference equation of state [25, 26], and the corresponding chromatographic peak area A_i was measured on the TCD. A slightly non-linear calibration relationship was then established by regression with the following equation:

$$\rho_i = \frac{n_i}{V} = a_{i,1} A_i + a_{i,2} A_i^2 . \quad (1)$$

Here, n_i is the amount of component i, and V is the volume of the sample loop. When applied to determine the composition of a mixture, the sample-loop volume cancels out and so a nominal value was adopted for the larger loop and the ratio of the two loop volumes was treated as an adjustable parameter such that the calibration data from the two different loops joined smoothly. Figure 2 illustrates the results of the calibration for (CO_2 + CH_4).

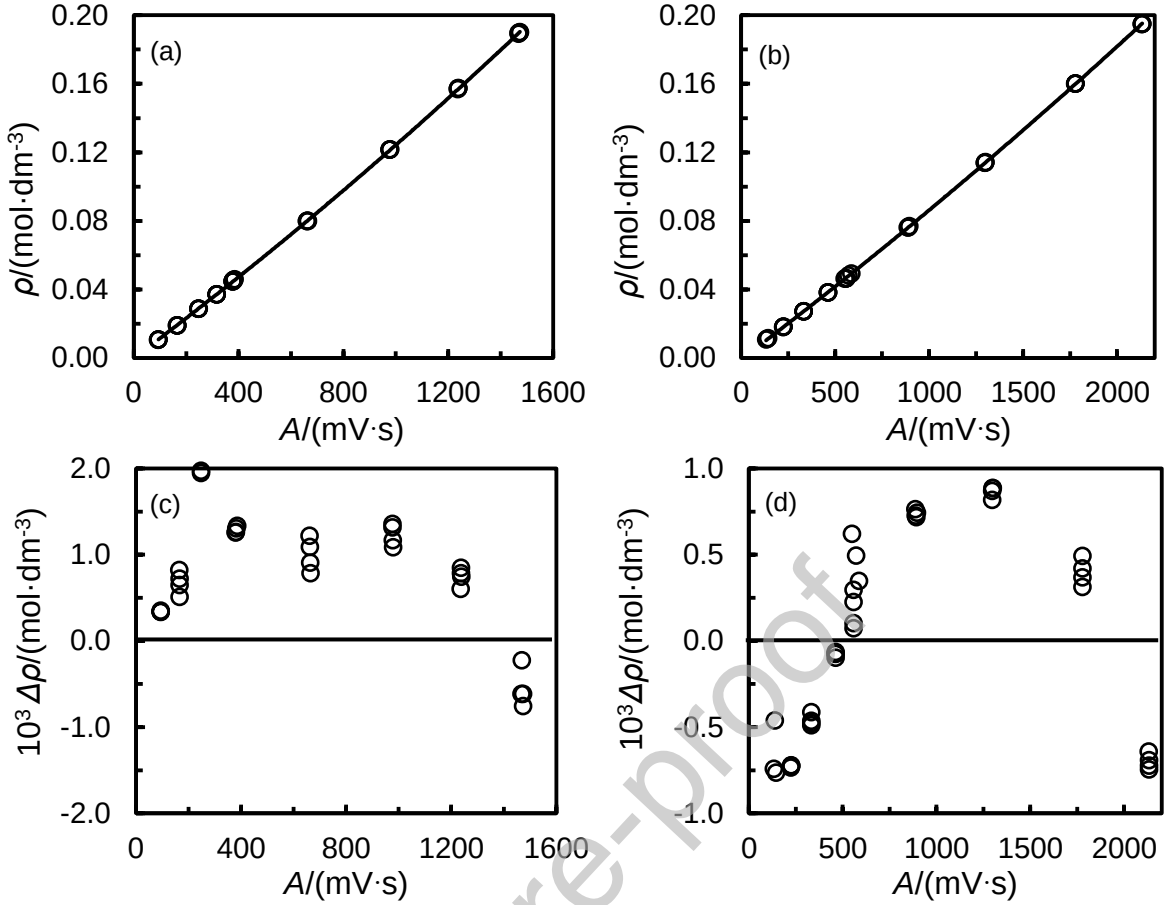

Figure 2. Thermal-conductivity detector calibration data for CH_4 (a and c) and CO_2 (b and d) with He carrier gas: (a) and (b), gas molar density ρ under filling-loop conditions against peak area response A; (c) and (d), deviations $\Delta\rho$ of gas molar density from Eq. (1) against area response A. O, experimental data; ——, Eq. (1).

As a validation of the method, we analyzed a standard test mixture $(1 - z)$ CO_2 + z CH_4, obtained from SIP Analytical with z = (0.0500 ± 0.0003); the composition determined by GC was z = (0.0503 ± 0.0024) where confidence intervals are based on one standard uncertainty.

In the case of H_2S, the sulfur-specific FPD was used which sources a current proportional to the square of the amount of sulfur in the sample. Calibration was carried out using a prepared mixture containing 10 ppm of H_2S in CH_4 and the results conformed to the following equation:

$$\rho_{H_2S} = \frac{n_{H_2S}}{V} = a_{H_2S}\sqrt{A}\,. \qquad (2)$$

Fig. 3(a) shows the calibration data gathered using the larger sample loop only. Given the very dilute nature of the test mixture, the density (concentration) of H_2S was taken to be the molar density of pure CH_4 multiplied by the mole fraction of H_2S. Fig. 3(b) shows the deviations of the calibration data from Eq.(1) and indicates satisfactory agreement. It should be noted that, since the objective was ultimately to determine a distribution coefficient for H_2S between coexisting liquid and vapor phases, we only required linearity of the relationship between n and $\sqrt{A}$.

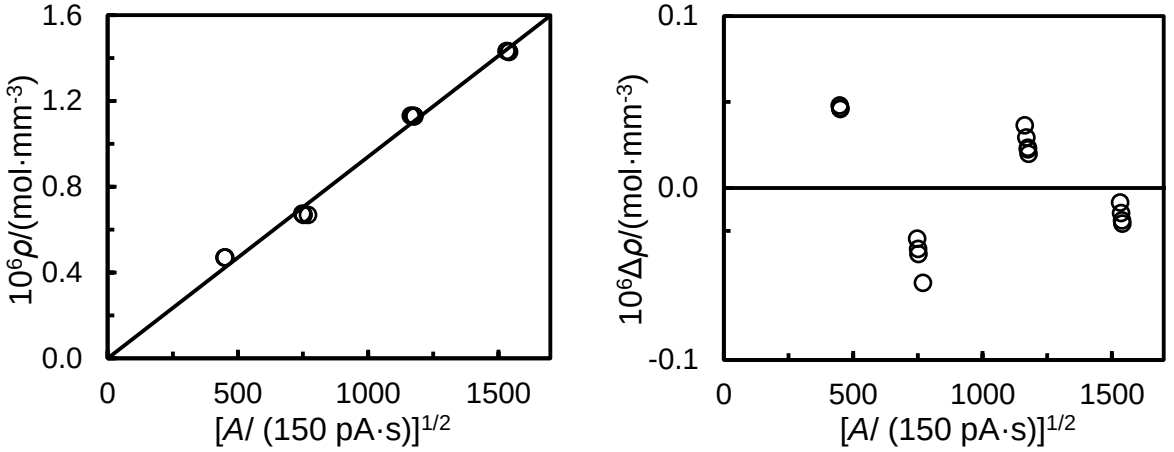

Figure 3. Flame photometric detector calibration data for H_2S with He carrier gas: (a) H_2S molar density ρ under filling-loop conditions against square root of the peak area response A; (b) deviations $\Delta\rho$ of H_2S molar density from Eq. (2) against area response A. O, experimental data; ——, Eq. (2).

The GC conditions were optimized to minimize the analytical runtime while assuring complete separation between the chromatographic peaks corresponding to the different components.

The experimental procedure for the binary VLE measurements was essentially identical to that described earlier for (CO_2 + H_2), (CO_2 + N_2) and (CO_2 + CO) systems [27, 28]. Measurements were conducted along isotherms. The initially clean and evacuated cell was first filled approximately one third to half full with pure CO_2. The equilibrium vapor pressure of the CO_2 was measured and compared with the equation of state (EoS) of Span and Wagner [26]. If the deviation of the vapor pressure from the EoS was within the combined uncertainty then the measurements continued; if not the sample was vented and the vessel subjected to further cycles of purging with CO_2 and evacuation. To increase the pressure along an isotherm, pure methane was admitted to the cell in increments. Following the establishment of equilibrium at each state point, as judged from the constancy of temperature and pressure, samples were taken alternately from the coexisting liquid and vapor phases. The first sample from each phase was always discounted and then, typically, five or six samples were analyzed for each phase. The VLE cell was not equipped with a window and the coexistence of liquid and vapor phases was verified by monitoring the composition of the samples withdrawn from the top and the bottom of the cell. In most cases, the initial CO_2 filling level was such that the liquid-vapor interface remained in between the two sampling locations up to the maximum pressure investigated on a given isotherm, as evidenced by the measured compositions. Only at the highest temperature investigated (303.15 K) was there any difficulty in ensuring that the measurements remained within the two-phase region; in that case it was necessary to try several initial filling levels.

The procedure for SVLE measurements was the same as described previously [27] and involved determining the three-phase temperature-pressure locus only without sampling.

For the ternary VLE measurements, a procedure similar to that for the binary mixture was followed. Three gas supplies were used during these measurements: pure CO_2, pure CH_4

and a mixture of 1000 ppm H_2S in CH_4. When increasing the pressure along an isotherm, gas mixture was injected along with additional pure CH_4 so as to establish a liquid-phase mole fraction of $H_2S \leq 40$ ppm. Samples were separated on the RT Sulfur column with CH_4 and CO_2 eluting first and passing directly to the TCD. After the CO_2 peak had eluted, a valve in the GC was switched to direct the column effluent to the FPD to allow the H_2S peak to be determined. The sample size taken was kept sufficiently small that the absolute amount of H_2S was within the range of the calibration. However, since just the ratio $K_3 = y_3/x_3$ was to be determined, we require only that the FPD signal obeyed Eq.(2); the value of the calibration coefficient a_{H_2S} was not required. Despite the use of sulfur-inert tubing, fittings and valves throughout, there was evidence of H_2S adsorption in the sampling system. We observed that the first few chromatographic peaks in a series of samples were smaller than expected. With repeated sampling, the peak areas became constant and the value of K_3 was repeatable from one sample to the next. Since the measurements were made on mixtures of different and unspecified overall composition, we report only the mole fractions of H_2S in the liquid phase and the corresponding values of K_3, effectively in the limit of infinite dilution.

SVLE measurements were carried out without sampling of the phases. Crossing of the three-phase equilibrium line, separating the regions of (vapor + liquid) and (solid + liquid) coexistence, was determined from isochoric pressure measurements during a slow cooling ramp as described previously by Fandiño et al. [27].

3. Results

3.1 VLE of the (CO_2 + CH_4) binary system

The VLE of the (CO_2 + CH_4) system was measured along seven isotherms at temperatures from (218.15 to 303.15) K at pressures from the vapor pressure of pure CO_2 to just below the mixture critical pressure. The experimental results obtained for both the vapor and the liquid phases are given in Table 3 in which the temperature T, pressure p and mole fractions x and y are the average of temperature, pressure and liquid or vapor mole fraction of CH_4 at each state point, based on replicated measurements. The corresponding standard uncertainties, calculated as detailed in reference [28], are also given in Table 3. The measured data are shown in Fig. 4 on a pressure-composition diagrams for all seven temperatures measured. There is an slight increase in the uncertainty in the mole fractions with increase in pressure. The highest composition uncertainties are generally in the proximity of the critical point on each isotherm as a consequence of the increased influence of the uncertainty in pressure.

Table 3. Experimental VLE data for CO_2 (1) + CH_4 (2) at temperature T and pressure p, where x_2 is the mole fraction of CH_4 in the liquid phase with standard uncertainty $u(x_2)$, and y_2 is the mole fraction of CH_4 in the vapor phase with standard uncertainty $u(y_2)$.[a]

T/K	p/MPa	x_2	y_2	$u_c(x_2)$	$u_c(y_2)$
218.124 [b]	0.5532	0.0000	0.0000	-	-
218.145	0.8732	0.0132	0.3468	0.0011	0.0027
218.180	1.1058	0.0237	0.4696	0.0007	0.0028
218.171	1.8213	0.0582	0.6546	0.0066	0.0025
218.169	2.8929	0.1218	0.7576	0.0012	0.0020

T/K	p/MPa	x_2	y_2	$u_c(x_2)$	$u_c(y_2)$
218.172	3.7838	0.1917	0.7963	0.0017	0.0018
218.160	4.6286	0.2919	0.8115	0.0023	0.0017
218.163	5.1122	0.3740	0.8162	0.0026	0.0017
218.151	5.3996	0.4287	0.8174	0.0027	0.0017
218.161	5.7312	0.5209	0.8157	0.0028	0.0017
218.161	5.8674	0.5588	0.8142	0.0027	0.0017
218.165	5.9578	0.5848	0.8126	0.0027	0.0017
218.162	6.0455	0.6099	0.8105	0.0026	0.0017
218.170	6.2832	0.6811	0.7970	0.0024	0.0018
218.162	6.3845	0.7245	0.7738	0.0022	0.0019
233.154 [b]	1.0040	0.0000	0.0000	-	-
233.160	1.3425	0.0141	0.2286	0.0008	0.0021
233.156	1.7737	0.0314	0.3955	0.0006	0.0027
233.156	2.8909	0.0862	0.5898	0.0009	0.0027
233.156	3.8581	0.1431	0.6639	0.0014	0.0025
233.158	4.6773	0.2028	0.6993	0.0018	0.0023
233.158	5.4856	0.2763	0.7180	0.0022	0.0022
233.160	5.9690	0.3314	0.7236	0.0025	0.0022
233.162	6.3499	0.3824	0.7245	0.0026	0.0022
233.163	6.7550	0.4449	0.7198	0.0027	0.0022
233.161	7.0343	0.4977	0.7104	0.0028	0.0023
233.159	7.2113	0.5360	0.6982	0.0028	0.0023
243.123 [b]	1.4287	0.0000	0.0000	-	-
243.160	1.7687	0.0133	0.1713	0.0006	0.0017
243.152	2.3978	0.0392	0.3552	0.0005	0.0026
243.152	3.1965	0.0760	0.4836	0.0008	0.0028
243.155	3.8823	0.1111	0.5495	0.0011	0.0027
243.154	4.8616	0.1694	0.6077	0.0016	0.0026
243.157	5.6499	0.2260	0.6348	0.0019	0.0026
243.150	6.9907	0.3551	0.6488	0.0025	0.0025
243.157	7.4730	0.4208	0.6376	0.0027	0.0026
243.158	7.8819	0.5101	0.5948	0.0028	0.0027
258.159 [b]	2.2923	0.0000	0.0000	-	-
258.157	2.6446	0.0162	0.1117	0.0005	0.0012
258.142	3.0422	0.0291	0.2047	0.0005	0.0018
258.151	4.1449	0.0769	0.3667	0.0008	0.0026
258.149	4.9488	0.1161	0.4363	0.0011	0.0027
258.148	5.7641	0.1613	0.4807	0.0015	0.0028
258.153	6.2466	0.1914	0.5003	0.0017	0.0028
258.154	6.7410	0.2240	0.5133	0.0019	0.0028
258.158	7.2125	0.2597	0.5205	0.0021	0.0028
258.152	7.5498	0.2922	0.5203	0.0023	0.0028

T/K	p/MPa	x_2	y_2	$u_c(x_2)$	$u_c(y_2)$
258.152	7.8400	0.3207	0.5156	0.0024	0.0028
258.157	8.0253	0.3511	0.5084	0.0025	0.0028
273.154 [b]	3.4840	0.0000	0.0000	-	-
273.145	3.6338	0.0056	0.0318	0.0003	0.0005
273.150	4.4255	0.0361	0.1606	0.0004	0.0015
273.146	5.3830	0.0769	0.2615	0.0008	0.0021
273.143	5.8701	0.0992	0.2980	0.0010	0.0023
273.145	6.3753	0.1245	0.3271	0.0012	0.0024
273.145	6.9351	0.1554	0.3506	0.0015	0.0025
273.149	7.0664	0.1625	0.3555	0.0015	0.0025
273.151	7.2102	0.1709	0.3590	0.0016	0.0025
273.153	7.4111	0.1845	0.3632	0.0017	0.0026
273.150	7.6710	0.2017	0.3668	0.0018	0.0026
273.156	7.9234	0.2210	0.3664	0.0019	0.0026
273.146	8.0407	0.2324	0.3636	0.0020	0.0026
273.152	8.2135	0.2495	0.3587	0.0021	0.0025
273.154	8.2957	0.2601	0.3526	0.0021	0.0025
288.155 [b]	5.0910	0.0000	0.0000	-	-
288.151	5.5641	0.0181	0.0563	0.0003	0.0006
288.137	6.0279	0.0367	0.1017	0.0004	0.0010
288.168	6.5109	0.0565	0.1389	0.0006	0.0013
288.156	6.7690	0.0684	0.1548	0.0007	0.0015
288.160	7.0385	0.0811	0.1694	0.0008	0.0016
288.161	7.2644	0.0922	0.1806	0.0009	0.0016
288.166	7.5583	0.1089	0.1899	0.0011	0.0017
288.153	7.6479	0.1146	0.1920	0.0011	0.0017
288.157	7.8325	0.1270	0.1944	0.0012	0.0017
288.158	7.9790	0.1395	0.1932	0.0013	0.0017
288.158	8.0795	0.1534	0.1874	0.0014	0.0017
303.166 [b]	7.2123	0.00000	0.00000	-	-
303.147	7.2363	0.00104	0.00171	0.00001	0.00002
303.147	7.2858	0.00336	0.00487	0.00004	0.00005
303.157	7.2925	0.00359	0.00516	0.00004	0.00006
303.156	7.3165	0.00466	0.00653	0.00018	0.00019
303.156	7.3649	0.00694	0.00908	0.00018	0.00019
303.157	7.3845	0.00795	0.01006	0.00019	0.00020

[a] Standard uncertainties are $u(T)$ = 0.006 K and $u(p)$ = 0.009 MPa. [b] CO_2 vapor pressure measurement.

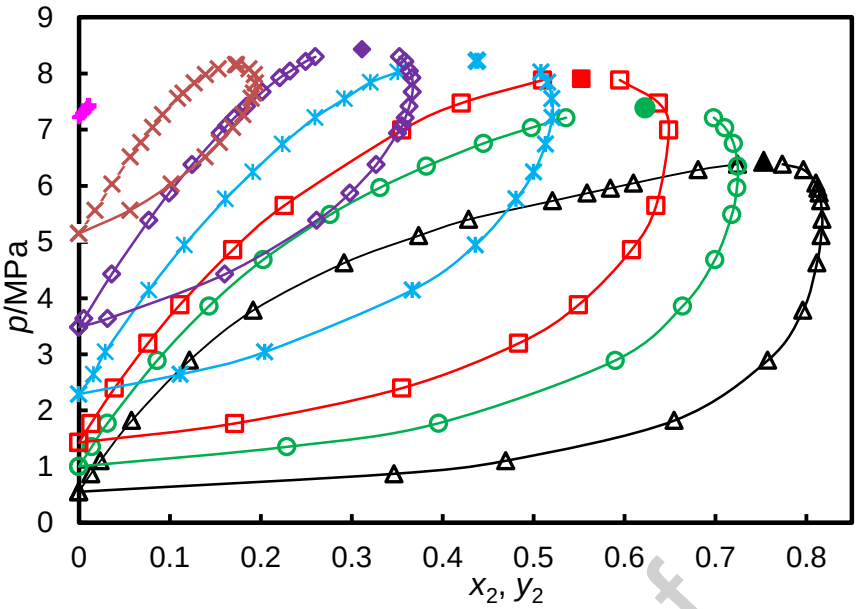

Figure 4. Pressure-composition diagram for CO_2 (1) + CH_4 (2) where p denotes pressure and x_2 and y_2 are mole fractions of CH_4 in the liquid and vapor phases, respectively. Open symbols denote experimental data and filled/bold symbols represent estimated critical points: △, T = 218.15 K; ○, T = 233.15 K; □, T = 243.15 K; ✳, T = 258.15 K; ◇, T = 273.15 K; ×, T = 288.15 K; +, T = 303.15 K. Lines are smooth curves to guide the eye.

3.2 Partition Coefficient of H_2S at High Dilution

Measurements of the partition coefficient $K_3 = y_3/x_3$ were made in the ternary mixture of CO_2 (1) + CH_4 (2) + H_2S (3) under conditions in which $x_3 \leq 4 \times 10^{-5}$. Under these conditions of high dilution, the gross phase behavior remains that of the (CO_2 + CH_4) binary mixture with a trace level of H_2S partitioned between the coexisting phases. Measurements were made on four isotherms over a range of pressures similar to that investigated for the binary and the mole fractions of each component were determined in both phases. It was verified that the K factors, $K_i = y_i/x_i$, of CO_2 and CH_4 in the coexisting phases were in agreement with those determined in the binary system and we report, in Table 4, the values of K_3 pertaining to H_2S. The standard relative uncertainties of K_3, which range from 2% to 4%, are dominated by the repeatability uncertainty of the composition measurements. With very small mole fractions to determine, this repeatability was less good than for the major components, despite the use of the highly-sensitive sulfur-specific FPD.

Table 4. Partition coefficients K_3 of H_2S in the CO_2 (1) + CH_4 (2) + H_2S (3) system at temperatures T and pressures p with standard uncertainties $u_c(K_3)$ and standard relative uncertainties $u_{c,r}(K_3)$. The corresponding values x_3 of the liquid-phase mole fraction of H_2S are also given. [a]

T/K	p/MPa	$10^6 x_3$	K_3	$u_c(K_3)$	$10^2 u_{c,r}(K_3)$
218.14	1.2294	4.7	0.481	0.011	2.3
218.14	2.4912	14.1	0.224	0.005	2.1
218.14	3.6964	19.9	0.224	0.005	2.1

218.14	4.9657	31.5	0.206	0.005	2.1
218.14	5.7826	27.8	0.448	0.010	2.1
218.14	6.2285	32.8	0.537	0.011	2.1
243.15	2.1546	3.6	0.702	0.016	2.3
243.15	2.9674	7.9	0.498	0.011	2.1
243.15	4.0887	16.3	0.395	0.008	2.1
243.15	4.3376	14.2	0.423	0.009	2.1
243.15	5.1673	15.8	0.623	0.013	2.1
243.15	6.0802	17.0	0.745	0.016	2.1
243.15	6.9366	17.2	0.829	0.017	2.1
243.15	7.5689	18.4	0.910	0.019	2.1
273.15	4.1553	2.7	0.782	0.022	2.7
273.15	5.3837	8.2	0.658	0.014	2.1
273.15	6.5935	12.4	0.667	0.014	2.1
273.15	7.2173	9.8	0.704	0.015	2.1
273.15	8.0060	11.6	0.777	0.016	2.1
288.16	5.4826	1.0	0.843	0.033	3.9
288.16	6.4449	2.9	0.881	0.020	2.3
288.16	6.8314	3.9	0.874	0.019	2.2
288.16	7.5736	4.9	0.892	0.019	2.1
288.16	7.6197	6.5	0.865	0.018	2.1
288.16	8.0132	7.1	0.936	0.020	2.1

[a] Standard uncertainties are $u(T)$ = 0.006 K, $u(p)$ = 0.009 MPa, and $u(x_3) = 1 \times 10^{-6}$.

3.3 SVLE of the (CO_2 + CH_4) binary system

Isochoric cooling ramps were carried out for various initial charging conditions. These were conducted at a controlled ramping rate of -1 K per hour starting at a temperature a few kelvin above the expected three-phase equilibrium state. Fig. 5 shows the results of a typical cooling ramp with pressure plotted against the temperature measured in the cell wall. There was a clear change in slope of pressure as a function of temperature in all cases and the three-phase state was determined by fitting quadratic polynomials to the pressure-temperature data in each region and solving for their intersection. Based on repeatability, the standard uncertainty of the intersection pressure at given temperature is estimated to be 0.035 MPa. The results are given in Table 5.

Table 5. Three-phase (solid + vapor + liquid) equilibrium points for (CO_2 + CH_4).[a]

T/K	*p*/MPa	*T*/K	*p*/MPa
203.96	4.858	210.67	3.655
207.07	4.691	214.16	1.981
209.58	4.101	215.79	0.964
209.63	4.104		

[a] standard uncertainty of equilibrium pressure at given temperature $u(p)$ = 0.035 MPa.

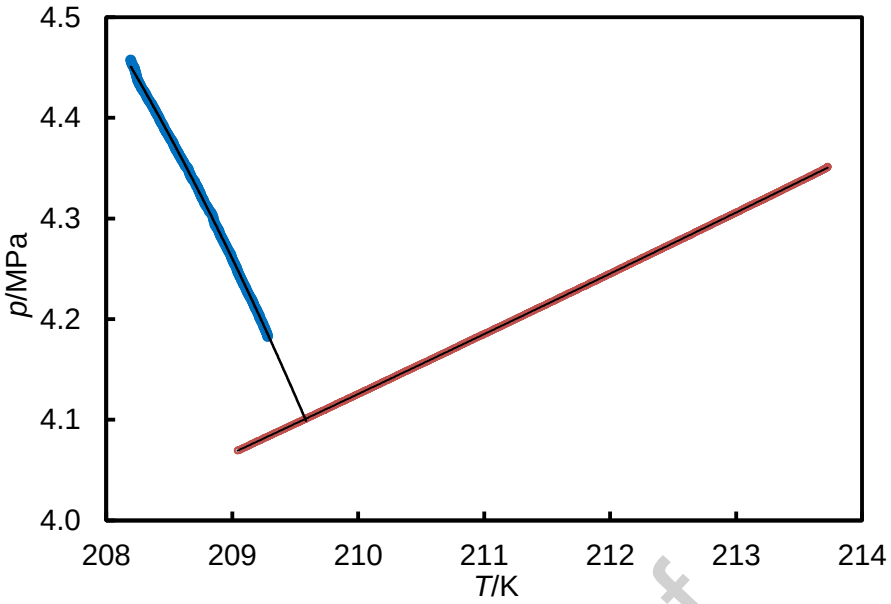

Figure 5. Pressure p as a function of cell temperature T during a cooling ramp at -1 K·h^{-1} in a mixture of CO_2 + CH_4. Symbols: red, (vapor + liquid) region; blue, (solid + liquid) region. Curves are quadratic polynomial fits.

4. Analysis and Discussion

4.1 The Critical Line of the (CO_2 + CH_4) System

The present VLE measurements extend close to the critical curve but critical points themselves were not directly observed. In order to determine the critical point on each isotherm precisely, the VLE data close to the critical pressure were fitted by the following scaling equation:

$$z_2 = z_{2,c} + \left(\lambda_1 + \varepsilon\frac{\lambda_2}{2}\right)(p_c - p) + \varepsilon\frac{\mu}{2}(p_c - p)^{\beta}. \quad (3)$$

Here, z_2 denotes the mole fraction of CH_4 on either the dew curve (ε = 1) or the bubble curve (ε = -1), $z_{2,c}$ is the critical composition, p_c is the critical pressure, β = 0.325 is the critical exponent and λ_1, λ_2 and μ are adjustable parameters. The critical mole fraction and pressure, as well as the three other adjustable parameters, were adjusted in a non-linear weighted least-squares optimisation to fit the experimental data in the critical region. The objective function for this optimisation was defined as follows:

$$S^2 = \sum_{i=1}^{N}\left[\left(\frac{x_2 - x_{2,\mathrm{calc}}}{u_c(x_2)}\right)^2 + \left(\frac{y_2 - y_{2,\mathrm{calc}}}{u_c(y_2)}\right)^2\right], \quad (4)$$

where N is the number of tie lines considered and $x_{2,\mathrm{calc}}$ and $y_{2,\mathrm{calc}}$ are bubble- and dew-point mole fractions of CH_4 calculated from the model. The isotherm at T = 303.15 K was not analysed in this way as the data do not extend close enough to the critical pressure. Fig. 6 shows the near critical data on each isotherm considered in comparison with Eq. (3) with the best fit parameters, which are given in Table 6.

Table 6. Parameters in equation (3)

T/K	p_c/MPa	$z_{2,c}$	λ_1	λ_2	μ
218.164	6.401	0.7523	-0.1215	-0.1924	-0.1864
233.161	7.372	0.6288	-0.0741	-0.0631	-0.2749
243.155	7.914	0.5542	-0.0566	-0.0496	-0.2543
258.155	8.358	0.4371	-0.0408	-0.0101	-0.2378
273.152	8.429	0.3116	-0.0357	-0.0047	-0.1772
288.156	8.155	0.1731	-0.0389	-0.0144	-0.0892

To establish correlations for the critical locus along its entire length, we consider the new results together with the recent high-precision measurements of Petropoulou et al. [24] and the well-known critical points of the pure components [25, 26]. We propose correlations for the critical pressure and mole fraction of CH_4 as functions of the dimensionless temperature $\theta = (T - T_{c,2}) / (T_{c,1} - T_{c,2})$ as follows:

$$p_c = \theta p_{c,1} + (1-\theta) p_{c,2} + \theta \left[a_{p,1}(1-\theta) + a_{p,2}(1-\theta)^2 + a_{p,3}(1-\theta)^3 \right] \quad (4)$$

$$z_{2,c} = 1 - \theta + \theta \left[a_{z,1}(1-\theta) + a_{z,2}(1-\theta)^2 + a_{z,3}(1-\theta)^3 \right] \quad (5)$$

The parameters of this model were fitted to the selected data, with $p_{c,1}$ and $p_{c,2}$ constrained to the pure-component values, and are given in Table 7, together with the standard uncertainties of the correlations.

Table 7. Parameters in equations (4) and (5) for the critical locus of (CO_2 + CH_4)

$a_{p,1}$/MPa	9.7615	$a_{z,1}$	0.25568
$a_{p,2}$/MPa	-2.3767	$a_{z,2}$	0.11129
$a_{p,3}$/MPa	3.1488	$a_{z,3}$	-1.43642
$a_{p,3}$/MPa	-8.4433	$a_{z,3}$	1.05271
$u(p_c)$/MPa	0.017	$u(z_c)$	0.0018

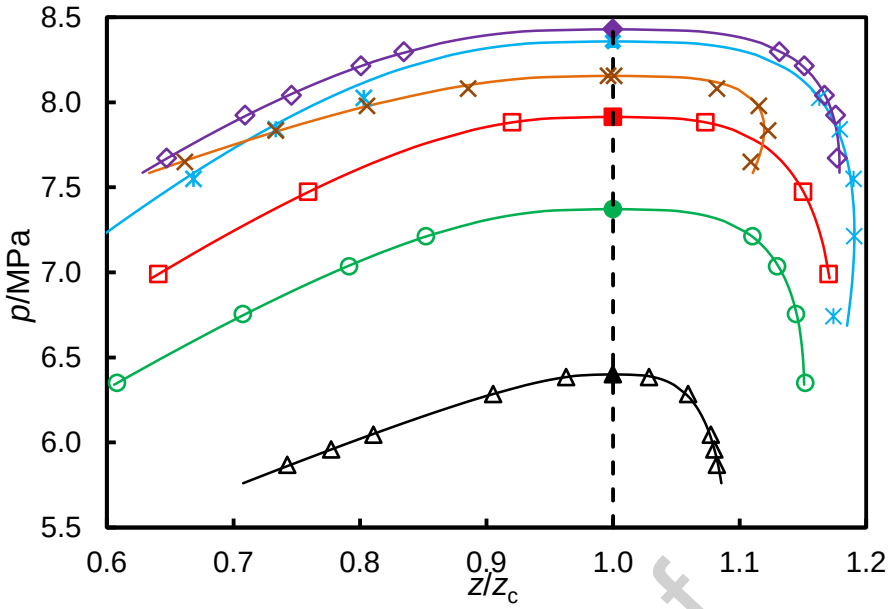

Figure 6. Pressure-composition diagram for CO_2 (1) + CH_4 (2) where p denotes pressure, z_2 denotes mole fractions of CH_4 on the dew and bubble curves and $z_{2,c}$ is the critical mole fraction of CH_4 on each isotherm. in the liquid and vapor phases, respectively. Open symbols denote experimental data and filled/bold symbols represent estimated critical points: △, T = 218.15 K; ○, T = 233.15 K; □, T = 243.15 K; ∗, T = 258.15 K; ◇, T = 273.15 K; ×, T = 288.15 K. Lines are calculated from Eq. (3) with parameters from Table 6. The dashed line indicated $z_2 = z_{2,c}$.

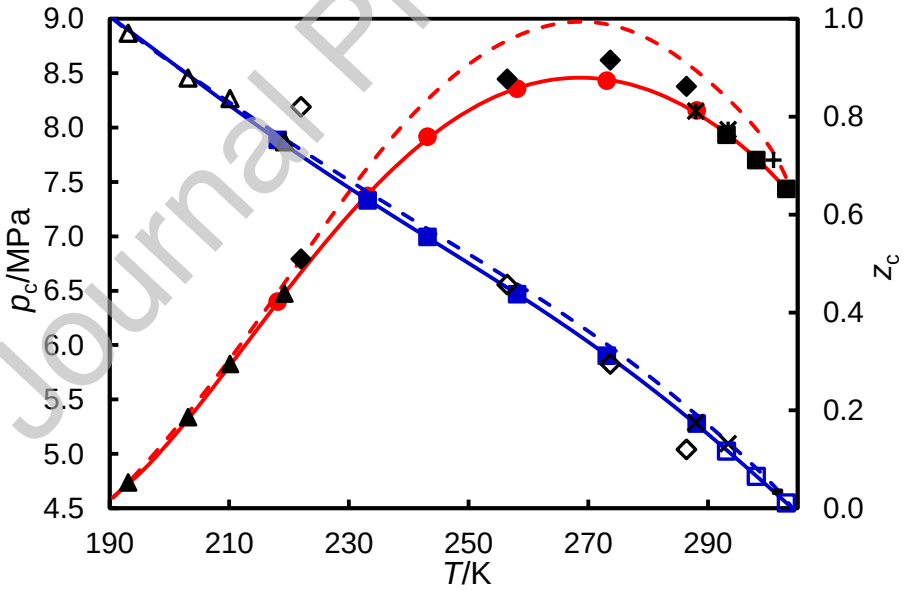

Figure 7. Critical pressure p_c and critical mole fraction $z_{2,c}$ for the CO_2 (1) + CH_4 (2) system as a function of temperature T. Critical pressure: ●, this work; ◆, ■, Petropoulou et al. [24]; Donnelly and Katz [1], ▲, Mraw et al. [10], ∗, Xu et al. [16];+, Bian et al. [18]. Critical temperature: ○, this work; □,Petropoulou et al. [24]; ◇, Donnelly and Katz [1]; △, Mraw et al. [10], ×, Xu et al. [16]; –, Bian et al. [18]. Solid lines represent equations (4) and (5). Dashed curves are calculated from the GERG-2008 mixture model [29] as implemented in REFPROP [30].

Fig. 7 compares the present results and data from the literature with the critical locus correlations. These correlations provides an excellent fit to the selected data (i.e. our results and those of Petropoulou et al. [24]) and the critical composition locus is also quite similar to that obtained from the GERG-2008 mixture model [29] as implemented in the REFPROP software package [30]. It should be noted that REFPROP implements more accurate pure-fluid equations of state than are specified in GERG-2008 but it has the same mixing terms. However, the GERG-2008 model seriously over estimates the critical pressure in the middle of the composition range. The new correlations are in fair agreement with most of the other literature data [1, 10, 16, 18], except for those of Donnelly and Katz [1], which are in poor agreement, and the critical pressure reported by Bian et al. [18] which appears to be too high.

4.2 Bubble and Dew Curves of the (CO_2 + CH_4) System

Direct comparisons with many of the previously-published VLE data are difficult because they pertain to different temperatures. However, in Fig. 8, we compare the present results with data from the literature where the isotherms coincident. Agreement with Knapp et al. [31] at T = 233.15 K and with the recent results of Petropoulou et al. [24] at T = 303.15 K is excellent, while the agreement with Arai et al. [8] and Xu et al. [16] at T = (273.15 and 288.15) K is quite

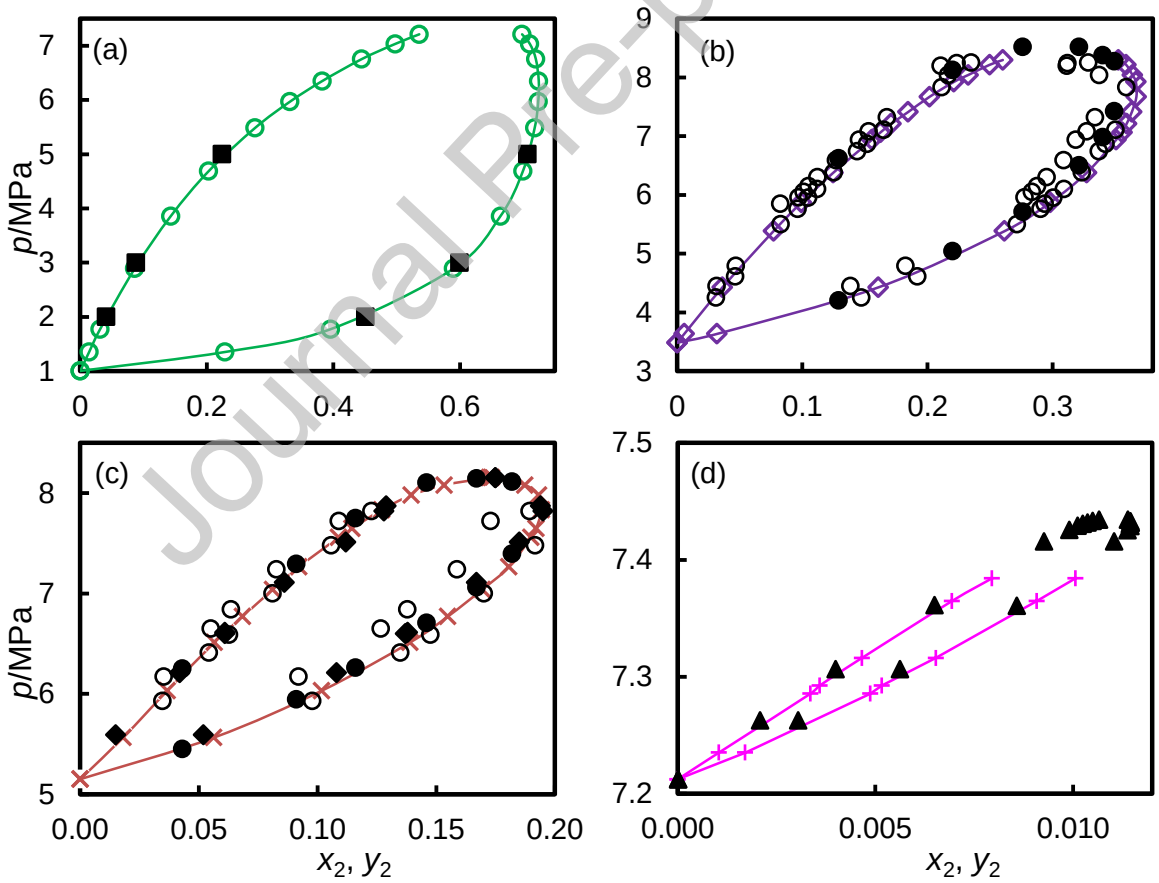

Figure 8. Pressure-composition diagrams for CO_2 (1) + CH_4 (2) where p denotes pressure and x_2 and y_2 are mole fractions of CH_4 in the liquid and vapor phases, respectively, at (a) T = 233.15 K, (b) T = (272.15 to 274.15) K, (c) T = (287.5 to 289.5) K , (d) T = 303.15 K. ○, ◇, ×, +, this work; ■, Knapp et al. [15]; ●, Arai et al. [8]; ◆, Xu et al. [16]; ○, Nasir et al. [23]; ▲, Petropoulou et al. [24].

satisfactory. One can observe that the methane mole fractions reported by Arai et al. are systematically lower than our result. In the case of Xu et al., their bubble-point compositions and critical presure are in good agreement with the present results but their dew-point methane mole fractions are again slightly lower than ours. On the other hand, the data reported by Nasir et al. [23] are quite scattered and in generally poor agreement with both the current work and other literature sources.

Table 8. Critical temperature T_c, critical pressure p_c and acentric factor ω of the pure components.

Components	T_c/K	p_c/MPa	ω	Ref.
CO_2	304.13	7.3773	0.22394	[26]
CH_4	190.56	4.5992	0.01142	[25]

We have modelled our data with the Peng-Robinson equation of state with classical one-fluid mixing rules and a single temperature-dependent binary interaction parameter k_{12}. The mathematical form of the PR-EoS is well known and not repeated here [32]. The pure-component properties required to evaluate the parameters in the model are the critical temperature T_c, critical pressure p_c and the acentric factor ω. Table 8 lists the values of these parameters.

The one remaining parameter, the binary interaction parameter k_{12}, was fitted to the experimental data by minimization of the objective function Φ define as follows:

$$\Phi^2 = \left[\frac{1}{N_x} \sum_{i=1}^{N_x} \left(\frac{x_{2,i,\mathrm{exp}} - x_{2,i,\mathrm{calc}}}{u(x_{2,i,\mathrm{exp}})} \right)^2 + \frac{1}{N_y} \sum_{i=1}^{N_y} \left(\frac{y_{2,i,\mathrm{exp}} - y_{2,i,\mathrm{calc}}}{u(y_{2,i,\mathrm{exp}})} \right)^2 \right]. \tag{6}$$

Here, $x_{2,i,\mathrm{exp}}$ and $y_{2,i,\mathrm{exp}}$ are i^{th} experimental mole fractions of CH_4 on the bubble and dew curves with standard uncertainties $u(x_{2,i,\mathrm{exp}})$ and $u(y_{2,i,\mathrm{exp}})$, respectively, $x_{2,i,\mathrm{calc}}$ and $y_{2,i,\mathrm{calc}}$ are the corresponding bubble- and dew-point compositions evaluated from the model at the same temperature and pressure, N_x is the number of bubble points and N_y is the number of dew points. Additionally, we define unweighted root-mean-square (RMS) deviations of bubble-point and dew-point compositions, S_x and S_y, where

$$\begin{aligned} S_x^2 &= N_x^{-1} \sum_{i=1}^{N} \left(x_{2,i,\mathrm{exp}} - x_{2,i,\mathrm{calc}} \right)^2 \\ S_y^2 &= N_y^{-1} \sum_{i=1}^{N} \left(y_{2,i,\mathrm{exp}} - y_{2,i,\mathrm{calc}} \right)^2, \end{aligned} \tag{7}$$

and an unweighted overall RMS deviation S such that

$$S^2 = \left(N_x + N_y \right)^{-1} \left(N_x S_x^2 + N_y S_y^2 \right). \tag{8}$$

The average deviations (bias) for bubble- and dew-point compositions, B_x and B_y, are also calculated as follows:

$$\begin{aligned} B_x &= N^{-1} \sum_{i=1}^{N} (x_{2,i,\mathrm{exp}} - x_{2,i,\mathrm{calc}}) \\ B_y &= N^{-1} \sum_{i=1}^{N} (y_{2,i,\mathrm{exp}} - y_{2,i,\mathrm{calc}}) \end{aligned} \tag{9}$$

Note that, for our data, N_x = N_y. Initially, k_{12} was fitted to the data for each isotherm individually. The isotherm at T = 303.15 K were not analyzed in this way as the limited amount of data at that temperature does not permit a sensitive adjustment. We found that the k_{12} values determined on each isotherm follow a smooth curve which we correlated as follows:

$$k_{12} = -0.99567 + 0.0023309(T / \mathrm{K}) + 126.45(\mathrm{K} / T) . \quad (10)$$

As expected from such a simple model, the representation of the VLE data is not perfect and the final value of the objective function Φ was 3.7, whereas this parameter would reduce to unity for an optimal fit. Fig. 9 shows the values of k_{12} determined on each isotherm in comparison with Eq. (10). Also shown are the values of k_{12} reported recently by Nasir et al. [23] and the values predicted by the E-PPR78 model of Xu et al. [33].

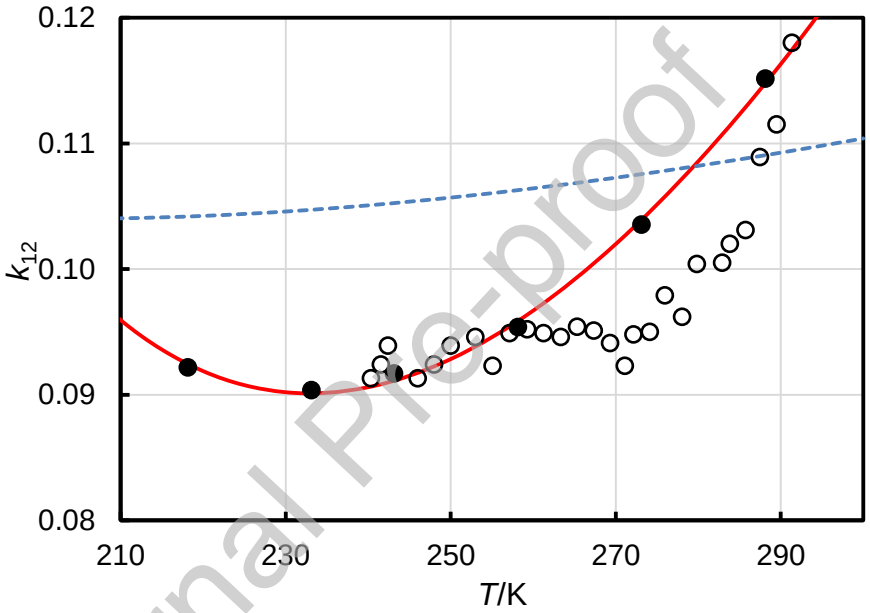

Figure 9. Binary interaction parameter k_{12} as a function of temperature T for (CO_2 + CH_4): ●, this work; O, Nasir et al. [23]; solid line, Eq. (10); dashed line, E-PPR78 model [33].

Fig. 10 compares the experimental VLE data (symbols) with the PR-EoS model (solid curves), and Table 9 summarizes the statistical measures defined above. The bias figures show that, on average, the model slightly underestimates the mole fraction of methane on the dew curve and the graphs show that this occurs mainly in the critical region. The PR-EoS systematically overestimates the critical pressures and this no doubt reflects the fact that, while the calculated data follow equation (3) in the critical region, the model exhibits a critical exponent β of 1/2 instead of about 1/3. The relative failure of the model in the critical region affects the fit as a whole; nevertheless the model is always quite close to the experimental data. Applying the value of k_{12} from Eq. (10) to the isotherm at T = 303.15 K also results in a very reasonable description of the data.

Table 9. Statistical comparison of experimental and calculated VLE data, where S is the overall root-mean-square (RMS) deviation of composition, S_x is the RMS deviation in bubble-point composition, S_y is the RMS deviation in dew-point composition, B_x is the bias (mean deviation) of bubble-point compositions and B_y is the bias of dew-point compositions.

Model	S	S_x	S_y	B_x	B_y
PR-EoS	0.0075	0.0069	0.0081	-0.0007	0.0046
GERG-2008	0.0126	0.0158	0.0081	0.0099	-0.0018

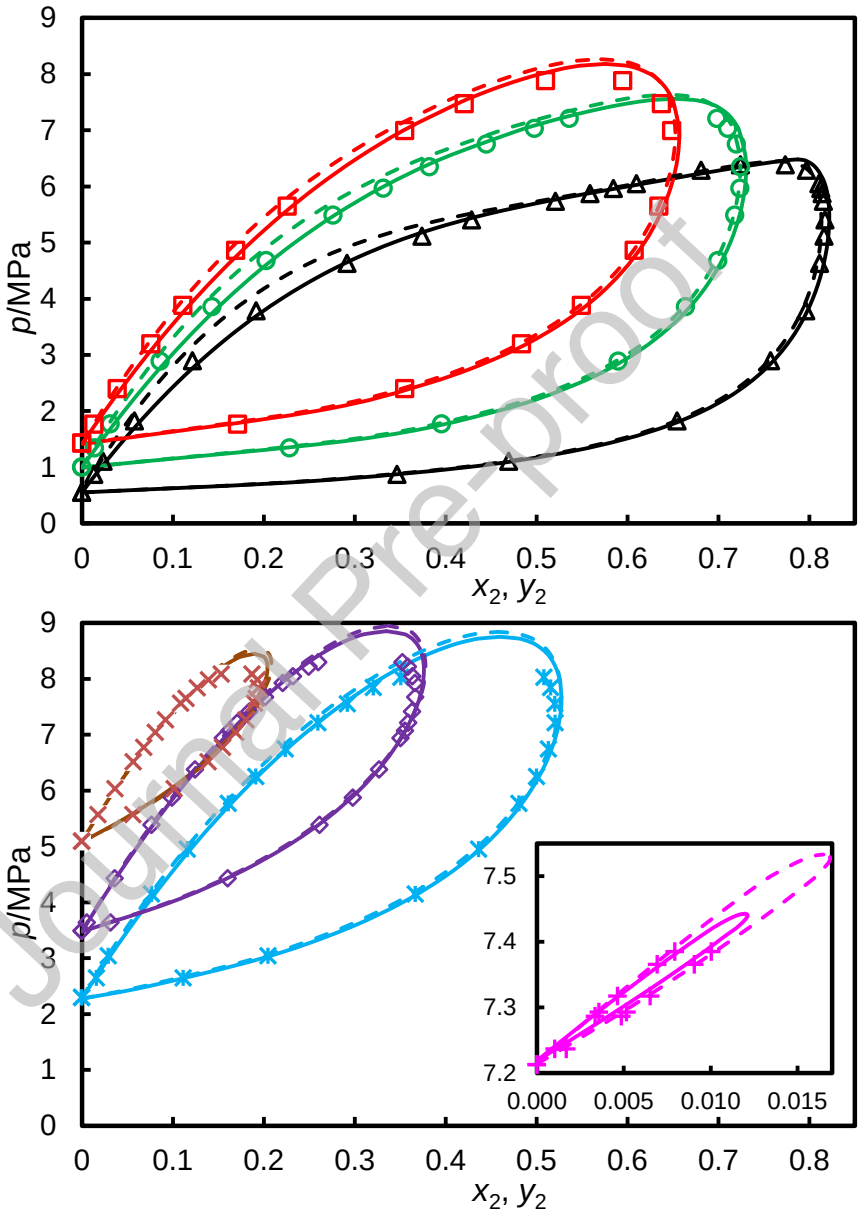

Figure 10. Pressure-composition diagrams for CO_2 (1) + CH_4 (2) where p denotes pressure and x_2 and y_2 are mole fractions of CH_4 in the liquid and vapor phases, respectively. Symbols denote experimental data: △, T = 218.15 K; ○, T = 233.15 K; □, T = 243.15 K; ✳, T = 258.15 K; ◇, T = 273.15 K; ×, T = 288.15 K; +, T = 303.15 K. Solid lines are calculated from the PR-EoS with the recommended binary interaction parameter. Dashed curves are calculated from the multi-fluid Helmholtz-energy approximation with the REFPROP software.

We also compare our VLE data with phase compositions evaluated from the GERG-2008 mixture model [29] as implemented in the REFPROP software [30]. The comparison is shown in Figure 10, there the GERG-2008 model is represented by dashed lines, and summarized statistically in Table 9. GERG-2008 is a much more sophisticated model than the PR-EoS and contains many parameters that were adjusted by its developers to fit a wide variety of mixture properties including densities, speeds of sound and VLE data. However, the principle aim of that fitting was to obtain the best possible representation of density in the so-called custody transfer regime. Perhaps as a result, the representation of VLE data is in fact slightly less good than that provided by the PR-EoS with k_{12} fitted to the data. This is reflected in the larger overall RMS deviation for the bubble-curve, along which mole fractions of CH_4 are generally under estimated, as reflected in the positive value of B_x; however, the dew curve is, on average, predicted slightly better than by the PR-EoS model. As noted in section 4.1, the GERG-2008 model overestimates the critical pressures and, at the higher temperatures considered here, this is significantly worse than with the PR-EoS.

A strength of the GERG-2008 framework is that it is capable to systematic improvement, either by adjusting the four binary reducing parameters that define the composition-dependent reduced temperature and density variables or, at a more comprehensive level, by developing a new binary-specific departure function. While the latter is beyond the scope of this work, the former was considered and it was found that the description of the VLE data could easily be improved by tuning the reducing parameters. However, to do this in a meaningful way, one must include in the analysis single phase properties, such as density and sound speed, otherwise the overall accuracy of the model will be compromised. When the present VLE data were considered along with high-accuracy density [34-36] and sound-speed [37] data no meaningful improvement in the overall representation could be achieved by means of manipulating any or all of the four reducing parameters. Therefore we conclude that an improved binary-specific departure function is required for this system.

4.3 Comparison of Literature Data with PR-EoS

In Table 10, we compare the available literature data, restricted to temperature above approximately 200 K, with the PR-EoS model with Eq. (10) for k_{12}, using the statistical metrics already defined. The different literature sources are sorted by the value of *S.* Excluding very small data sets, we note that the results of Petropoulou et al. [24], Bian et al. [18], Knapp et al. [15], Kaminishi et al. [5], Ahmad et al. [22] and Xu et al. [16] all show excellent agreement with the model, with overall RMS deviations $S < 0.01$. Other literature sources with $S < 0.02$ are Bian [17], Webster and Kidnay [20], Wei et al. [19], Somait and Kidnay [11], Davalos et al. [9], Toriumi and Kaminishi [6], Al-Sahhaf et al. [12], Mraw et al. [10], Nasir et al. [23] and Arai et al. [8]. As noted already, the dew-point data of Nasir et al. [23] are quite scattered ($S_y = 0.0256$) but, on average, they show good agreement with the model as evidenced by the bias metrics. The remaining data sets [1, 3, 7, 14] show greater scatter and/or systematic deviations from the model.

Table 10. Statistical comparison of literature VLE data with compositions calculated from the PR-EoS with binary parameters from Eq. (10), where T_{min} and T_{max} are the minimum and maximum temperatures considered for each data set, S_x is the root-mean-square (RMS) deviation in bubble-point composition, S_y is the RMS deviation in dew-point composition, B_x is the bias (mean deviation) of bubble-point compositions and B_y is the bias of dew-point compositions.

T_{min}/K	T_{max}/K	N_x	N_y	S	S_x	S_y	B_x	B_y	Author(s)	Ref.
241.5	241.5	1	1	0.0029	0.0031	0.0026	-0.0031	-0.0026	Hensel & Massoth	[4]
293.1	303.2	34	34	0.0055	0.0023	0.0074	0.0000	0.0001	Petropoulou et al.	[24]
301.0	301.0	26	26	0.0058	0.0050	0.0065	0.0000	0.0000	Bian et al.	[18]
201.1	222.6	1	5	0.0061	0.0047	0.0064	0.0047	-0.0001	Pikaar	[2]
220.0	223.2	7	7	0.0070	0.0085	0.0052	0.0010	0.0007	Knapp et al.	[15]
277.8	302.2	11	11	0.0076	0.0089	0.0060	-0.0006	0.0000	Ahmad et al.	[22]
233.2	283.2	14	14	0.0076	0.0056	0.0091	0.0000	0.0004	Kaminishi et al.	[5]
288.5	293.4	21	21	0.0082	0.0091	0.0072	-0.0003	-0.0001	Xu et al.	[16]
258.2	258.2	1	1	0.0092	0.0030	0.0126	0.0030	0.0126	Freitag & Robinson	[13]
293.0	298.1	6	6	0.0095	0.0066	0.0117	-0.0003	0.0019	Bian	[17]
230.0	270.0	39	38	0.0098	0.0065	0.0123	0.0000	0.0002	Webster & Kidnay	[20]
230.0	270.0	49	49	0.0114	0.0090	0.0133	0.0000	0.0002	Wei et al.	[19]
270.0	270.0	9	12	0.0116	0.0084	0.0135	-0.0002	0.0007	Somait & Kidnay	[11]
230.0	270.0	33	34	0.0126	0.0105	0.0143	-0.0001	-0.0001	Davalos et al.	[9]
283.2	293.2	13	13	0.0129	0.0088	0.0159	0.0001	0.0004	Toriumi & Kaminishi	[6]
219.3	270.0	27	29	0.0136	0.0114	0.0153	-0.0001	0.0003	Al-Sahhaf et al.	[12]
203.2	219.3	23	12	0.0141	0.0172	0.0036	0.0004	0.0003	Mraw et al.	[10]
240.4	297.2	259	259	0.0192	0.0089	0.0256	0.0000	0.0001	Nasir et al.	[23]
253.2	288.2	11	23	0.0196	0.0138	0.0219	0.0001	0.0007	Arai et al.	[8]
199.8	271.5	68	63	0.0284	0.0309	0.0255	0.0002	-0.0002	Donnelly & Katz	[1]
208.5	219.9	23	23	0.0343	0.0401	0.0274	-0.0008	-0.0006	Neumann & Walch	[7]
277.6	277.6	1	1	0.0360	0.0021	0.0508	-0.0021	-0.0508	Robinson et al.	[3]
205.4	256.2	4	5	0.0552	0.0420	0.0638	0.0006	0.0054	Esper at al.	[14]

Fig. 11 shows a more detailed analysis of the deviations for each data set containing 7 or more points (the results report by Bian and Bian et al. [17, 18] are treated as a single data set). Here, for each data set and separately for bubble and dew points, the distributions of mole-fraction deviations are summarised by the minimum and maximum deviations, and the lower quartile, median, mean and upper quartile deviations excluding outliers. Outliers are points that fall more than 1.5 times the interquartile range above the upper quartile or below the lower quartile, based on the remaining data. These outliers are shown individually and often occur in the critical region where, as noted above, the PR-EoS model does not exhibit the correct scaling. Based on Figure 11, the most consistent data sets appear to be: Xu et al. [16], Bian and Bian et al. [17, 18], Webster & Kidnay [20], Ahmad et al. [22], Petropoulou et al. [24] and the present work. Each of these data sets shows small deviation in both liquid and vapor phases with few outliers.

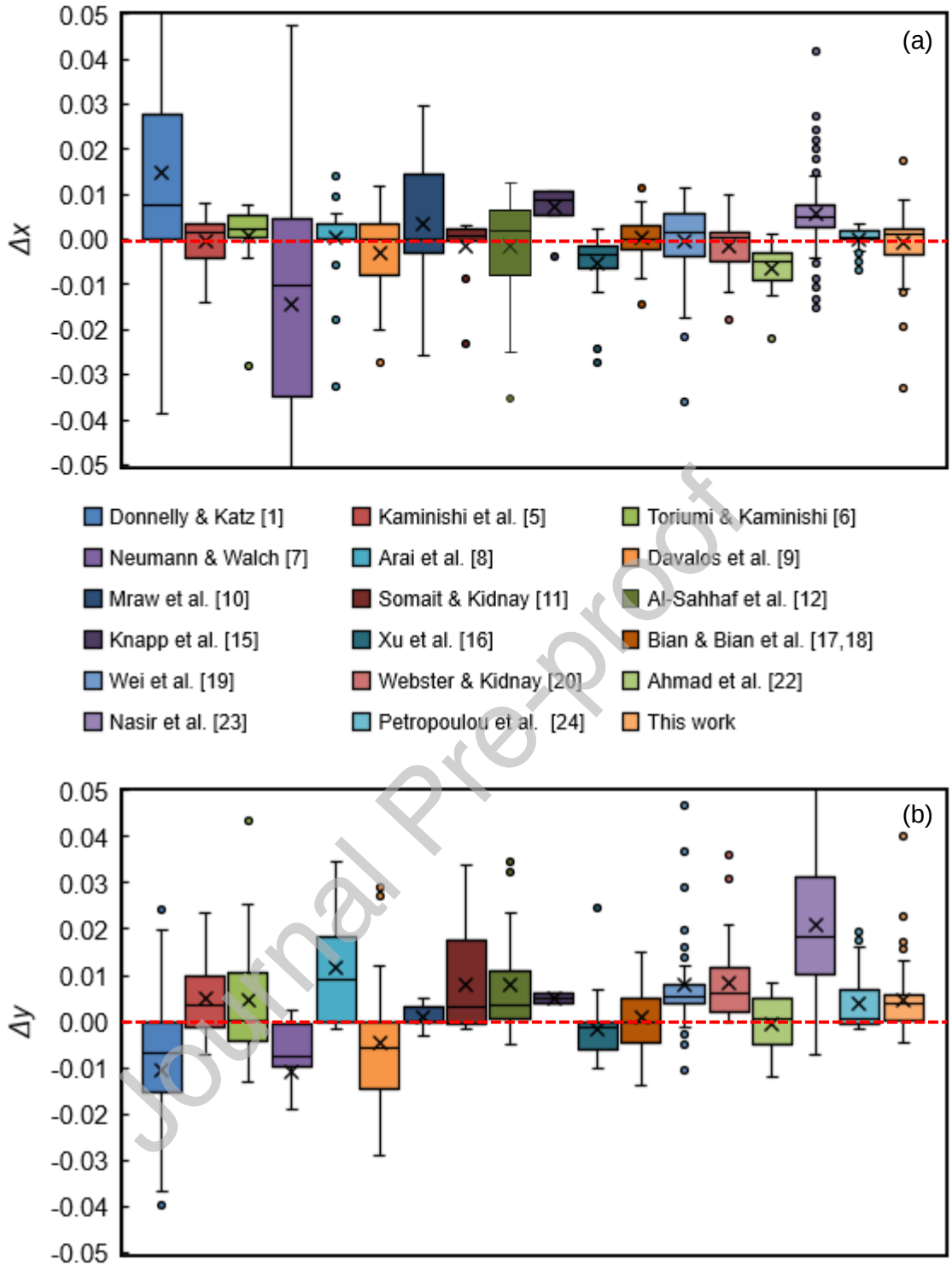

Figure 11. Box-plot comparison between experimental phase compositions for CO_2 (1) + CH_4 (2) with the predictions of the Peng-Robinson equation of state, categorized by author: (a) deviations $\Delta x = x_{exp} - x_{calc}$ of bubble-point compositions and (b) deviations $\Delta y = y_{exp} - y_{calc}$ of dew-point compositions, where subscripts 'exp' and 'calc' denote experimental and calculated values, respectively. For each data set, the lower and upper edges of the box mark the lower and upper quartile deviations, respectively, the horizontal line through the box marks the median deviation and the symbol (×) marks the mean deviation (bias). The vertical bars show the span from the minimum to maximum deviation, excluding points (O) identified as outliers.

4.4 H_2S Partition Coefficients

The partition coefficients $K_3 = y_3/x_3$ of H_2S measured in the (CO_2 + CH_4 + H_2S) ternary system are plotted as a function of pressure in Fig. 12. The solid curves in Fig. 12 were computed from the PR-EoS for H_2S at infinite dilution in (CO_2 + CH_4) making use of binary interaction parameters determined from experimental VLE data. For (CO_2 + CH_4) we used Eq. (10) while, in the case of (CO_2 + H_2S), we analyzed the VLE data reported by Hirata et al. [38], Ferrell et al. [39] and Chapoy et al. [40] and represented k_{13} as follows:

$$k_{13} = 0.1091 - 3.27 \cdot (\mathrm{K}/T) \tag{11}$$

Finally, for (CH_4 + H_2S) we used the temperature-dependent expression determined by Coquelet et al. [41]:

$$k_{23} = 0.0390 + 12.30 \cdot (\mathrm{K}/T) \tag{12}$$

With increasing pressure along an isotherm, starting from the vapor pressure of pure CO_2, the general trend is an initial reduction in K_3 as CH_4 is added to the mixture, until a turning point is reached and K_3 increases towards unity at the critical point. This same trend is clearly illustrated by the curves calculated from the PR-EoS, although the critical pressures predicted by that model deviate slightly from experiment. The results show that, in the ternary system at low temperatures and intermediate pressures, H_2S is quite strongly absorbed into the liquid phase, with some K_3 values as low as 0.2. The experiments are in generally-good agreement with the PR-EoS predictions. However, the results at T = 243.15 K and $p \geq 5.17$ MPa are a notable exception and do not follow the predictions of the PR-EoS. We have no explanation for this and can only add that the experimental data were repeatable within the stated uncertainty.

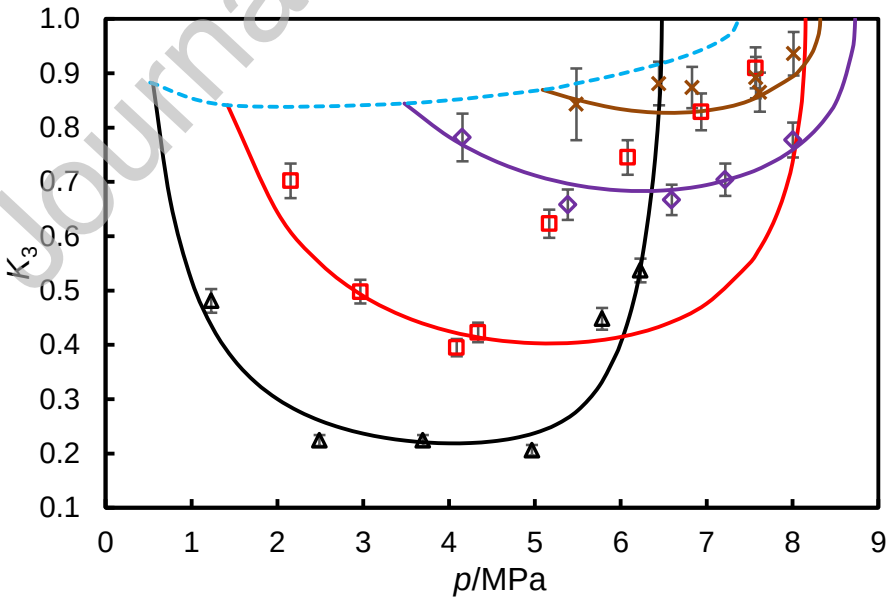

Figure 12. Partition coefficient $K_3 = y_3/x_3$ for highly-dilute H_2S in the CO_2 (1) + CH_4 (2) + H_2S (3) ternary system as a function of pressure p, where x and y denote mole fractions in the liquid and vapor phases, respectively. Experiment: △, T = 218.15 K; □, T = 243.15 K; ◇, T = 273.15 K; ×, T = 288.15 K. Error bars indicate the 95% confidence interval. Lines

calculated from the PR-EoS for H_2S at infinite dilution: solid line, H_2S in (CO_2 + CH_4); dashed line, H_2S in pure CO_2.

Fig. 12 also shows the partition coefficient computed from the PR-EoS for H_2S at infinite dilution in pure CO_2; this is the locus of end points for the ternary isotherms and runs from the triple point to the critical point of CO_2.

A few studies of the phase equilibria of the (CO_2 + CH_4 + H_2S) ternary system have been reported [3, 4, 42-44], although none of these address the high dilution behavior of H_2S and so only limited comparisons are possible. Hensel et al. [4] investigated mainly H_2S-rich mixtures but included a few states at T = 222.15 K with $x_3 \leq 0.18$, finding K_3 = (0.225, 0.170 and 0.224) at p = (2.07, 3.45 and 4.83) MPa, respectively. These values agree with our results at T = 218.15 K and similar pressures to within about 10%. For mixtures richer in H_2S, Hensel et al. [4] observed slightly smaller values of K_3 at the same pressures and temperatures. Ng et al. [43] investigated the phase behavior of the mixture (0.1 CO_2 + 0.5 CH_4 + 0.4 H_2S) and observed liquid-liquid-vapor equilibria at low temperatures terminating, for that particular composition, at a critical point located at T = 215.65 K and p = 6.62 MPa. Phase compositions were not analyzed. Recently, Theveneau et al. [44] reported VLE measurements with full composition analysis for two different global compositions at temperatures between (243.50 and 333.13) K and pressures up to 11.24 MPa. However, in their study, x_3 varied between 0.427 and 0.986 and so comparisons are not meaningful.

4.5 Solid-Vapor-Liquid Equilibrium Curve

The SVLE results reported here map the three-phase boundary from just above the triple-point pressure of pure CO_2 to near to the maximum pressure on the SVLE curve. The only data previously available in this region were those of Donnelly and Katz [45], which are scattered and appear to be of low quality. On the other hand, Davis et al. [45] and Pikaar [2] report extensive data along the lower-temperature branch of the SVLE curve. We have analyzed the data from this work and from those two previous studies to obtain an empirical correlation for the SVLE pressure-temperature locus. This was constructed in terms of dimensionless temperature and pressure variables defined by

$$\tau = (T - T_{t,2})/(T_{t,1} - T_{t,2}) \tag{13}$$

$$\varphi = \left[p - \tau p_{t,1} - (1-\tau) p_{t,2} \right] / p_{t,1}, \tag{14}$$

where subscript t indicates a property at a pure-component triple-point. The form of the correlation, arrived at by trial, is as follows:

$$\varphi = \exp\left[A + B\tau + C\tau^2 + D\tau^3 - \tau_0 (1-\tau)^{-n} \right], \tag{15}$$

and this fits the available data with standard uncertainty of 0.066 MPa. The values of the parameters are given in Table 11 and Fig. 13 compares the experimental data with the empirical model. The model is validated for temperatures between 143 K and the triple point temperature of CO_2. Although it reduces smoothly to the triple-point of CH_4 at 90.69 K, the model has not been validated against experimental measurements in this region.

Table 11. Parameters in Eq.(13) for the SVLE Locus

A	*B*	*C*	*D*	τ_0	*N*
9.614	34.028	-40.517	20.667	17.727	0.06

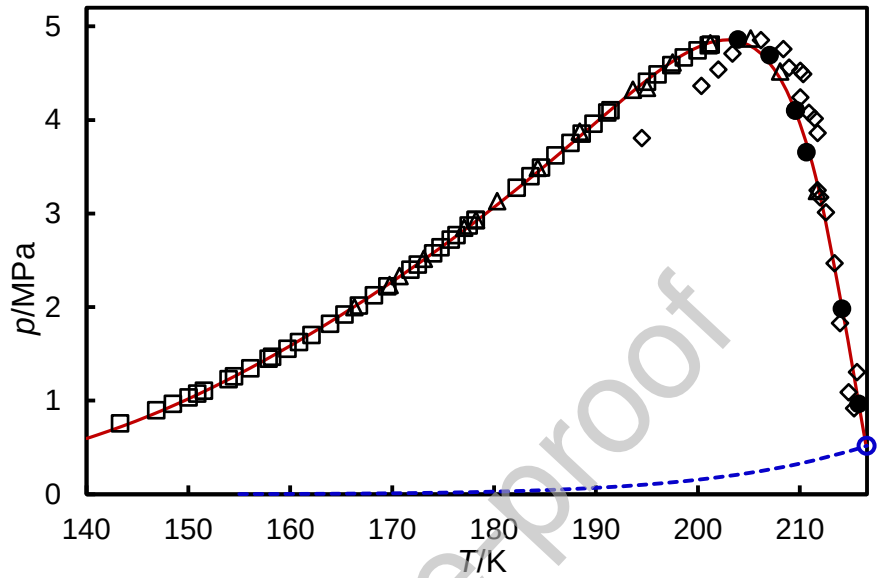

Figure 13. SVLE locus for the (CO_2 + CH_4) system where *T* is temperature and *p* is pressure: ●, this work; □, Pikaar [2]; Davis et al. △, [45]; ◇, Donnelly and Katz [1]; ○, triple point of CO_2. The solid curve is calculated from equation (15) with parameters from table 11. The dashed curve is the sublimation curve of CO_2.

5. Conclusions

The principal contribution of this work is a new set of precise VLE data for (CO_2 + CH_4) spanning almost the whole temperature range from the triple point to the critical point of CO_2, We have compared the VLE results directly and indirectly with a large body of existing literature data and identified several sources with which there is close agreement. Our results and these literature data should be helpful in devising improved thermodynamic models for the (CO_2 + CH_4) binary system, especially within the formalism of GERG-2008. Our work also determines the vapor-liquid critical locus more accurately than previously possible and provides new data and a precise empirical correlation for the three-phase SVLE locus. Finally, we provide new data and modelling for the partitioning of the important acid-gas impurity H_2S between liquid and vapor phases in the (CO_2 + CH_4) system under conditions of high dilution.

Acknowledgement

The authors are grateful to the CNPq for the award of a research scholarship, under the Brazilian scholarship program *Ciência sem Fronteiras* during the tenure of which this work was carried out.

Author Credit Statement

Lorena F. S. Souza: Methodology, Validation, Formal analysis, Investigation, Writing-original draft, Visualization.

Saif Z. S. Al Ghafri: Methodology, Investigation, Supervision, Writing – review & editing.

Olivia Fandiño: Methodology, Validation, Formal analysis, Investigation

J P Martin Trusler: Conceptualization, Methodology, Formal analysis, Writing – review & editing, Supervision

Declaration of interests

The authors declare that they have no known competing financial interests or personal relationships that could have appeared to influence the work reported in this paper.

References

[1] H.G. Donnelly, D.L. Katz, Phase Equilibria in the Carbon Dioxide-Methane System, Ind. Eng. Chem., 46 (1954) 511-517.

[2] M.J. Pikaar, A study of phase equilibria in hydrocarbon-CO_2 systems, PhD Thesis, University of London, 1959.

[3] D.B. Robinson, A.P. Lorenzo, C.A. Macrygeorgos, The carbon dioxide-hydrogen sulphide-methane system: Part I. Phase behavior at 100°F, Can. J. Chem. Eng., 35 (1959) 151-158.

[4] W.E. Hensel, F.E. Massoth, Phase Equilibria for the Ternary System: CH_4-CO_2-H_2S, J. Chem. Eng. Data, 9 (1964) 352-356.

[5] G.-I. Kaminishi, Y. Arai, S. Saito, S. Maeda, Vapor-Liquid Equilibria for Binary and Ternary Systems Containing Carbon Dioxide, J. Chem. Eng. Jpn., 1 (1968) 109-116.

[6] T. Toriumi, G. Kaminishi, Studies on the Vapor-Liquid Equilibria at High Pressures, Asahi Garasu Kogyo Gijutsu Shoreikai Kenkyu Hokoku, 14 (1968) 67-79.

[7] A. Neumann, W. Walch, Dampf/Flüssigkeits-Gleichgewicht CO_2/CH_4 im Bereich tiefer Temperaturen und kleiner CO_2-Molenbrüche, Chem. Ing. Tech., 40 (1968) 241-244.

[8] Y. Arai, G.I. Kaminishi, S. Saito, The Experimental Determination of the *pVTx* Relations for the Carbon Dioxide and the Carbon Dioxide-Methane Systems, J. Chem. Eng. Jpn., 4 (1971) 113-122.

[9] J. Davalos, W.R. Anderson, R.E. Phelps, A.J. Kidnay, Liquid-vapor equilibria at 250.00 K for systems containing methane, ethane, and carbon dioxide, J. Chem. Eng. Data, 21 (1976) 81-84.

[10] S.C. Mraw, S.-C. Hwang, R. Kobayashi, Vapor-liquid equilibrium of the methane-carbon dioxide system at low temperatures, J. Chem. Eng. Data, 23 (1978) 135-139.

[11] F.A. Somait, A.J. Kidnay, Liquid-vapor equilibriums at 270.00 K for systems containing nitrogen, methane, and carbon dioxide, J. Chem. Eng. Data, 23 (1978) 301-305.

[12] T.A. Al-Sahhaf, A.J. Kidnay, E.D. Sloan, Liquid + vapor equilibriums in the nitrogen + carbon dioxide + methane system, Ind. Eng. Chem. Fund., 22 (1983) 372-380.

[13] N.P. Freitag, D.B. Robinson, Equilibrium phase properties of the hydrogen—methane—carbon dioxide, hydrogen—carbon dioxide—n-pentane and hydrogen—n-pentane systems, Fluid Phase Equilib., 31 (1986) 183-201.

[14] G.J. Esper, D.M. Bailey, J.C. Holste, K.R. Hall, Volumetric Behavior of near-Equimolar Mixtures for CO_2+CH_4 and CO_2+N_2, Fluid Phase Equilib., 49 (1989) 35-47.

[15] H. Knapp, X. Yang, Z. Zhang, Vapor-liquid equilibria in ternary mixtures containing nitrogen, methane, ethane and carbon dioxide at low temperatures and high pressures, Fluid Phase Equilib., 54 (1990) 1-18.

[16] N. Xu, J. Dong, Y. Wang, J. Shi, High pressure vapor liquid equilibria at 293 K for systems containing nitrogen, methane and carbon dioxide, Fluid Phase Equilib., 81 (1992) 175-186.

[17] B. Bian, Measurement of Phase Equilibria in the Critical Region and Study of Equation of State, PhD Thesis, Nanjing Institute of Chemical Technology, 1992.
[18] B. Bian, Y. Wang, J. Shi, E. Zhao, B.C.Y. Lu, Simultaneous determination of vapor-liquid equilibrium and molar volumes for coexisting phases up to the critical temperature with a static method, Fluid Phase Equilib., 90 (1993) 177-187.
[19] M.S.W. Wei, T.S. Brown, A.J. Kidnay, E.D. Sloan, Vapor + Liquid Equilibria for the Ternary System Methane + Ethane + Carbon Dioxide at 230 K and Its Constituent Binaries at Temperatures from 207 to 270 K, J. Chem. Eng. Data, 40 (1995) 726-731.
[20] L.A. Webster, A.J. Kidnay, Vapor−Liquid Equilibria for the Methane−Propane−Carbon Dioxide Systems at 230 K and 270 K, J. Chem. Eng. Data, 46 (2001) 759-764.
[21] T.T. Shen, T. Gao, W.S. Lin, A.Z. Gu, Determination of CO_2 Solubility in Saturated Liquid CH_4 + N_2 and CH_4 + C_2H_6 Mixtures above Atmospheric Pressure, J. Chem. Eng. Data, 57 (2012) 2296-2303.
[22] M. Ahmad, J. Gernert, E. Wilbers, Effect of impurities in captured CO_2 on liquid-vapor equilibrium, Fluid Phase Equilib., 363 (2014) 149-155.
[23] Q. Nasir, K.M. Sabil, K.K. Lau, Measurement of isothermal (vapor+liquid) equilibria, (VLE) for binary (CH4+CO2) from T=(240.35 to 293.15) K and CO2 rich synthetic natural gas systems from T=(248.15 to 279.15) K, J. Nat. Gas Sci. Eng., 27 (2015) 158-167.
[24] E. Petropoulou, E. Voutsas, S.F. Westman, A. Austegard, H.G.J. Stang, S.W. Løvseth, Vapor - liquid equilibrium of the carbon dioxide/methane mixture at three isotherms, Fluid Phase Equilib., 462 (2018) 44-58.
[25] U. Setzmann, W. Wagner, A New Equation of State and Tables of Thermodynamic Properties for Methane Covering the Range from the Melting Line to 625 K at Pressures up to 100 MPa, J. Phys. Chem. Ref. Data, 20 (1991) 1061-1155.
[26] R. Span, W. Wagner, A new equation of state for carbon dioxide covering the fluid region from the triple-point temperature to 1100 K at pressures up to 800 MPa, J. Phys. Chem. Ref. Data, 25 (1996) 1509-1596.
[27] O. Fandino, J.P.M. Trusler, D. Vega-Maza, Phase behavior of (CO_2 + H_2) and (CO_2 + N_2) at temperatures between (218.15 and 303.15) K at pressures up to 15 MPa, Int. J. Greenhouse Gas Control, 36 (2015) 78-92.
[28] L.F.S. Souza, S.Z.S. Al Ghafri, J.P.M. Trusler, Measurement and modelling of the vapor-liquid equilibrium of (CO_2 + CO) at temperatures between (218.15 and 302.93) K at pressures up to 15 MPa, J. Chem. Thermodyn., 126 (2018) 63-73.
[29] O. Kunz, W. Wagner, The GERG-2008 wide-range equation of state for natural gases and other mixtures: an expansion of GERG-2004, J. Chem. Eng. Data, 57 (2012) 3032–3091.
[30] E.W. Lemmon, I.H. Bell, M.L. Huber, M.O. McLinden, NIST Standard Reference Database 23: Reference Fluid Thermodynamic and Transport Properties-REFPROP, Version 10.0, in, National Institute of Standards and Technology, Gaitherburg, 2018.
[31] U. Waterling, D.Q. Zheng, H. Knapp, Vapor-Liquid-Equilibria at High-Temperatures and Pressures in Binary-Mixtures Containing H_2, CH_4 and CO_2 with High Boiling Hydrocarbons - Experimental Equipment and Results, Chem. Eng. Process., 29 (1991) 155-164.
[32] D.-Y. Peng, D.B. Robinson, A new two-constant equation of state, Ind. Eng. Chem. Fundam., 15 (1976) 59-64.
[33] X. Xu, J.-N. Jaubert, R. Privat, P. Arpentinier, Prediction of Thermodynamic Properties of Alkyne-Containing Mixtures with the E-PPR78 Model, Ind. Eng. Chem. Res., 56 (2017) 8143-8157.
[34] T. El Hawary, Messung der Dynamischen Viskosität und der Dichte von Vier Erdgasgemischen für Drücke bis 15 MPa und Temperaturen bis 373 K in Einer Kombinierten Viskositäts-Dichte-Messapparatur, PhD Thesis, Rurh-Universitat Bochum, 2003.
[35] P. Claus, R. Kleinrahm, W. Wagner, Density Measurements on Ethane and Propane In the Temperature Range From 340 K to 520 K at Pressures up to 30 MPa, in, Ruhr-Universitat Bochum, Bochum, 2001.
[36] C.-A. Hwang, G.A. Iglesias-Silva, J.C. Holste, K.R. Hall, B.E. Gammon, K.N. Marsh, Densities of Carbon Dioxide + Methane Mixtures from 225 K to 350 K at Pressures up to 35 MPa, J. Chem. Eng. Data, 42 (1997) 897-899.

[37] J.F. Estela-Uribe, Equation of State for Natural Gas Systems, PhD Thesis, University of London, 1999.
[38] M. Hirata, S. Ohe, K. Nagahama, Computer aided data book of vapor-liquid equilibria, Kodansha Limited, Tokyo, 1975.
[39] J.K. Ferrell, R.W. Rousseau, D.G. Bass, The Solubility of Acid Gases in Methanol, in, North Carolona State University, Raleigh, N. Carolina, 1979.
[40] A. Chapoy, C. Coquelet, H.F. Liu, A. Valtz, B. Tohidi, Vapour-liquid equilibrium data for the hydrogen sulphide (H_2S) + carbon dioxide (CO_2) system at temperatures from 258 to 313 K, Fluid Phase Equilib., 356 (2013) 223-228.
[41] C. Coquelet, A. Valtz, P. Stringari, M. Popovic, D. Richon, P. Mougin, Phase equilibrium data for the hydrogen sulphide plus methane system at temperatures from 186 to 313 K and pressures up to about 14 MPa, Fluid Phase Equilib., 383 (2014) 94-99.
[42] D.B. Robinson, A.P. Lorenzo, C.A. Macrygeorgos, The carbon dioxide-hydrogen sulphide-methane system: Part II. Phase behavior at 40°F and 160°F, Can. J. Chem. Eng., 37 (1959) 212-217.
[43] H.J. Ng, D.B. Robinson, A.D. Leu, Critical Phenomena in a Mixture of Methane, Carbon-Dioxide and Hydrogen-Sulfide, Fluid Phase Equilib., 19 (1985) 273-286.
[44] P. Theveneau, X. Xu, O. Baudouin, J.-N. Jaubert, P. Ceragioli, C. Coquelet, Vapor–Liquid Equilibria of the CH4 + CO2 + H2S Ternary System with Two Different Global Compositions: Experiments and Modeling, J. Chem. Eng. Data, 65 (2020) 1802-1813.
[45] J.A. Davis, N. Rodewald, F. Kurata, Solid-liquid-vapor phase behavior of the methane-carbon dioxide system, AIChE J., 8 (1962) 537-539.

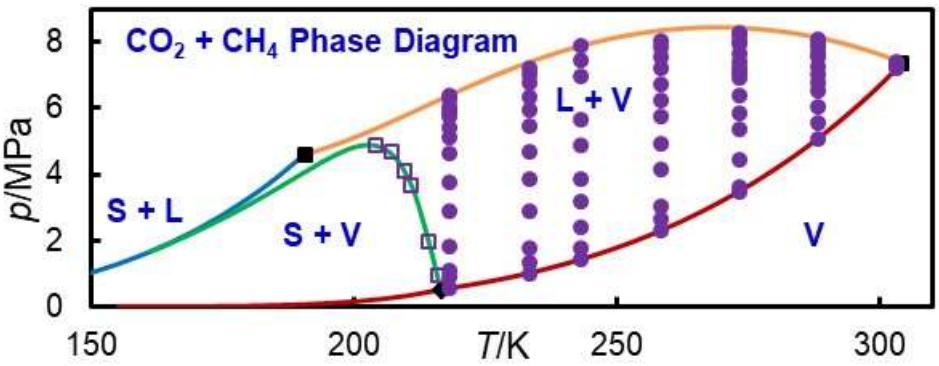

Graphical abstract for Table of Contents only.